J Appl Electrochem (2011) 41:123–127
DOI 10.1007/s10800-010-0210-y

ORIGINAL PAPER

Evaluation of corrosion behaviour of Ti–25Mo alloy in chloride medium

Satendra Kumar · T. S. N. Sankara Narayanan

Received: 22 December 2009 / Accepted: 6 September 2010 / Published online: 30 September 2010

Abstract The corrosion behaviour of Ti–25Mo alloy in 0.9 wt% NaCl was evaluated by potentiodynamic polarization, electrochemical impedance spectroscopy (EIS) and compared with that of commercially pure titanium (CP-Ti). The corrosion behaviour of Ti–25Mo alloy has been reported for the first time in this paper. The microstructure and structural characteristics were also examined using optical microscopy and X-ray diffraction (XRD), respectively. The study reveals that Ti–25Mo alloy possesses a β-phase microstructure. The Ti–25Mo alloy exhibits higher passivation range, lower average passive current density (i_{pass}) and higher charge transfer resistance (R_{ct}) compared to that of CP-Ti. Based on the corrosion protection ability, Ti–25Mo alloy can be a suitable alternative material for orthopaedic implant applications.

Keywords Ti–25Mo alloy · Corrosion · Polarization · Electrochemical impedance spectroscopy (EIS)

1 Introduction

Titanium and its alloys are widely used for orthopaedic and dental implants due to their low density, excellent biocompatibility, corrosion resistance and mechanical properties [1, 2]. Commercially pure titanium (CP-Ti) exhibits α-phase at room temperature. Recently, mechanical biocompatibility of biomaterials is also regarded as an important criterion in the selection of biomaterial. Hence, the research and development on β-type titanium alloys, which are considered advantageous in terms of mechanical biocompatibility, are increasing. Since the β-phase in Ti alloys exhibits a significantly lower modulus than the α-phase, the development of low modulus β-Ti alloys which retain a single β-phase microstructure on rapid cooling from high temperatures assumes significance. Several β-phase Ti alloys, having Nb, Ta, Zr and Mo as alloying elements (β-stabilizer elements) such as, Ti–12Mo–6Zr–2Fe and Ti–13Mo–7Zr–3Fe, Ti–15Mo–5Zr–3Al, Ti–15Mo–3Nb–3O, Ti–14Nb–13Zr, Ti–35Nb–7Zr–5Ta and Ti–34Nb–9Zr–8Ta, Ti–29Nb–4.6Zr–13Ta, Ti–15Mo, etc., were developed.

In case of Ti–Mo alloys, alloying of Ti with Mo leads to the formation of a dual phase ($\alpha + \beta$ phase) alloy at room temperature. When the Mo content of the Ti–Mo is increased more than 10 wt%, only the β-phase dominates. In recent years, Ti–Mo alloys have received considerable attention in terms of their better mechanical properties, corrosion resistance and biocompatibility for biomedical applications [3–14]. Ho [3, 4], Nag et al. [5, 6] and Oliveira et al. [7] have studied the structure and properties of a series of binary Ti–Mo alloy with Mo content ranging up to 20 wt%. Ti–Mo alloys offered a better corrosion resistance than CP-Ti in simulated physiological media. Oliveira et al. [7] and Oliveira and Guastaldi [8, 9] have reported that Ti–Mo alloys having 4–20 wt% Mo exhibit spontaneous passivation in Ringer's solution and they do not exhibit pitting at potentials up to 8 V (vs. SCE), indicating their excellent corrosion resistance. Besides, addition of Mo to the Ti alloy has been shown to improve the stability of the anodic oxides formed on these alloys [10, 11]. Karthega et al. [12] have reported that the corrosion resistance of Ti–15Mo and Ti–29Nb–13Ta–4.6Zr (TNTZ) (β-titanium alloys) in Hank's solution are almost similar. Alves et al. [13] have reported that the corrosion resistance offered by

S. Kumar · T. S. N. Sankara Narayanan (✉)
National Metallurgical Laboratory, CSIR Madras Complex, Taramani, Chennai 600 113, India
e-mail: tsnsn@rediffmail.com

Ti–10Mo alloy in fluoridated physiological serum is relatively better than that of Ti–6Al-4 V alloy. Based on the corrosion resistance, Capela et al. [14] have ranked CP-Ti and Ti–Mo alloys in the following order: CP-Ti < Ti–6.5Mo <Ti–8.5Mo < Ti–10Mo. Ti–15Mo alloy has been recommended for orthopaedic and dental implant applications in our previous studies [15, 16]. Hence, it is evident that Ti–Mo alloys can be considered as a candidate material for orthopaedic and dental implant applications. However, the corrosion behaviour of Ti–25Mo alloy has not been reported earlier. Hence, the present study aims to evaluate the corrosion behaviour of Ti–25Mo alloy in 0.9 wt% NaCl and to compare its corrosion performance with that of CP-Ti. The corrosion behaviour of Ti–25Mo alloy has been reported for the first time in this paper.

2 Materials and methods

CP-Ti (Grade 2) (Composition in wt%: Fe: 0.20; O: 0.18: N: 0.01; C: 0.03; H: 0.010: Ti: Balance) and Ti–25Mo alloy (in wt%: Fe: 0.17; O: 0.15: N: 0.02; C: 0.03; H: 0.011; Mo: 25.07; Ti: Balance) were used as the materials in the present study. CP-Ti was purchased from M/s Ti-Anode, Chennai, India. Ti–25Mo alloy was provided as a gift sample from National Institute of Material Research (NIMS), Japan. Ti–25Mo alloy was prepared in the form of a small button (10 mm ∅ and 5 mm thickness) by melting commercially pure titanium (grade one) and pieces of pure molybdenum (99.9%) in an arc melting furnace (with a W alloy electrode) under an ultra high pure argon atmosphere. Subsequently, the Ti–25Mo alloy buttons were annealed at 950 °C under high vacuum for 1 h and quenched in water to enable homogeneity and a β-phase microstructure. Samples for corrosion testing ($\sim$1 mm thick) were cut from these buttons. The microstructure of CP-Ti and Ti–25Mo alloy was examined using a Leica DMLM optical microscope with image analyzer software. The details of metallographic sample preparation were already reported in our earlier papers [15, 16]. The structural characteristics of CP-Ti and Ti–25Mo alloy were evaluated by X-ray diffraction (XRD) measurements, using Cu-Kα radiation. The corrosion behaviour of CP-Ti and Ti–25Mo alloys in 0.9 wt% NaCl was evaluated by potentiodynamic polarization and electrochemical impedance spectroscopy (EIS) studies using a potentiostat/galvanostat of ACM instruments (model: Gill AC). The choice of this electrolyte was made based on the earlier published reports [13–15, 17]. The details of sample preparation, electrode assembly, reference and counter electrodes were given in our earlier paper [15]. The potentiodynamic polarization and EIS studies were repeated at least 3 times to ensure reproducibility of the test results.

3 Results and discussion

3.1 Microstructure and structural characteristics

The microstructure of CP-Ti (Fig. 1) exhibits a typical rapidly cooled metastable feather-like microstructure that consists of equiaxed α-grain with some twin bands (indicated by arrow marks in Fig. 1). In contrast, β-grains are the only dominant phase in Ti–25Mo alloy in which the β-grains are homogeneous and evenly distributed (Fig. 1).

The retention of β-phase in Ti alloys with higher Mo content has also been reported earlier by Davis et al. [18]. Ho et al. [3] have reported that Ti–Mo alloys having 9 wt% Mo have a significant amount of equiaxed β-phase whereas in alloys containing $\geq$10 wt% Mo, the β-phase becomes the only dominant phase. Bania [19] has reported that a minimum of 10 wt% Mo is needed to fully stabilize β-phase at room temperature. The grain size of CP-Ti and Ti–25Mo alloy are in the range of 30–40 μm and 60–70 μm, respectively. The XRD pattern of CP-Ti is comprised entirely of hexagonal α-phase whereas β-phase is the only dominant phase in Ti–25Mo alloy (Fig. 2). Ho et al. [3] and Oliveira et al. [7] have confirmed a significant retention of the β-phase for the Ti alloy containing 10 wt% Mo, while in alloys having higher than 10 wt% Mo only the β-phase is retained, which is in agreement with the results of the present study.

3.2 Potentiodynamic polarization studies

The potentiodynamic polarization curves of CP-Ti and Ti–25Mo alloy in 0.9 wt% NaCl are quite similar in shape (Fig. 3). The anodic branch of the polarization curves of both CP-Ti as well as Ti–25Mo alloy exhibits spontaneous passivation. The open circuit potential (OCP), passivation range and passive current density are given in Table 1. CP-Ti exhibits passivation in the potential range from +145 to +1522 mV vs. SCE whereas Ti–25Mo alloy offers a relatively larger passive range, i.e. from +50 to 2530 mV vs. SCE in 0.9 wt% NaCl. The average passive current densities (i_{pass}) of CP-Ti and Ti–25Mo alloy are 32 ± 3 and 10 ± 5 μA cm^{-2}, respectively, which suggests the better corrosion protective ability of Ti–25Mo compared to that of CP-Ti. The results of the present study further confirm the observations made by other researchers on the corrosion protective ability of Ti–Mo alloys [7–9, 13–15].

3.3 Electrochemical impedance studies

The Nyquist plots of CP-Ti and Ti–25Mo alloy in 0.9 wt% NaCl recorded at their respective OCP's vs. SCE, are shown in Fig. 4. The Nyquist plot of CP-Ti (Fig. 4a) exhibits two semicircles, which indicates the involvement

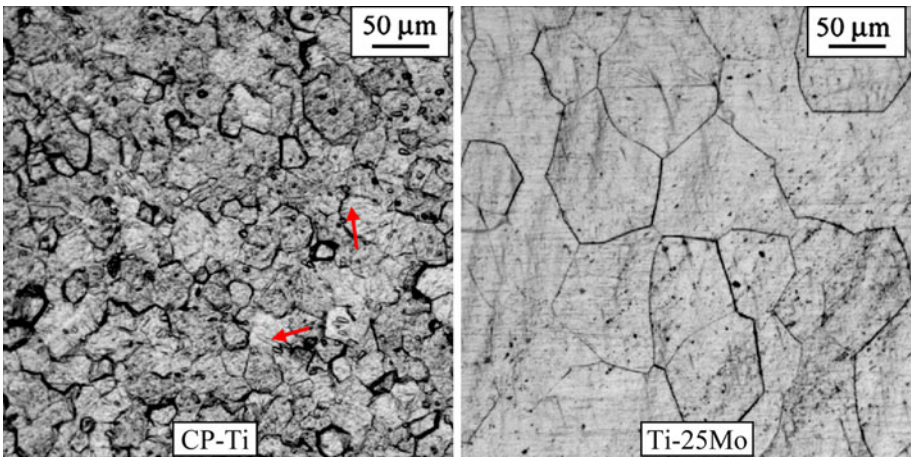

Fig. 1 Microstructures of CP-Ti and Ti–25Mo alloy

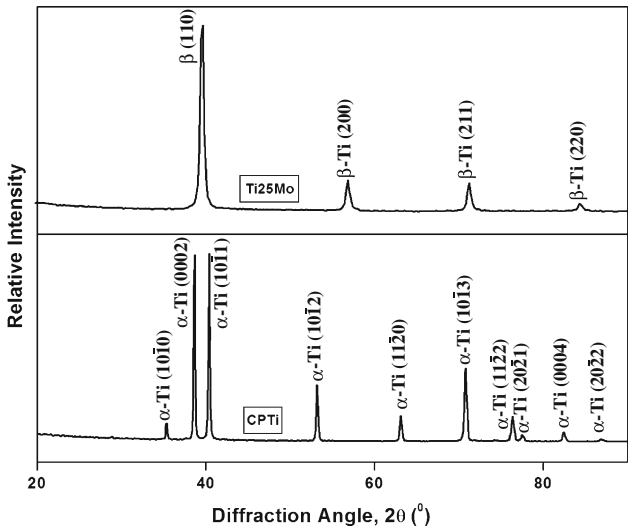

Fig. 2 X-ray diffraction patterns of CP-Ti and Ti–25Mo alloy recorded using Cu Kα radiation

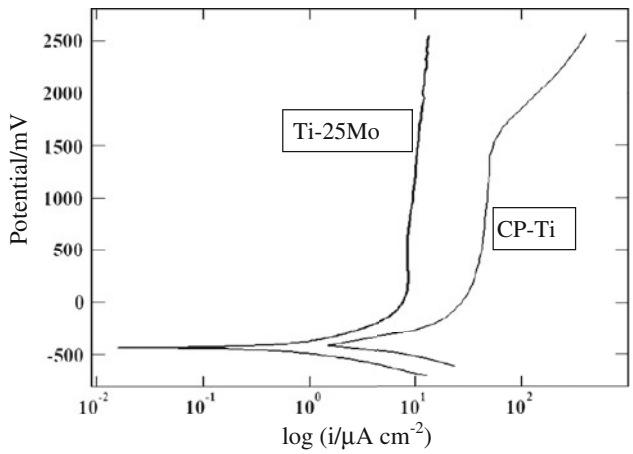

Fig. 3 Potentiodynamic polarization curves of CP-Ti and Ti–25Mo alloy in 0.9 wt% NaCl (*Potential range* −250 to +3000 mV with respect to the open circuit potential vs. SCE; *Scan rate* 100 mV min^{-1})

of two time constants. In contrast, the Nyquist plot of Ti–25Mo alloy (Fig. 4b) is characterized by a single semicircle, suggesting the involvement of single time constant. Two different equivalent electrical circuit models are used to analyze the EIS spectra of CP-Ti and Ti–25Mo alloy using Boukamp software. The fittings obtained for the EIS data along with the corresponding equivalent electrical circuit (EEC) are shown along with the experimental data in Fig. 4. In these two EEC, R_s represents the solution resistance and a constant-phase element (CPE) representing a shift from an ideal capacitor was used instead of the capacitance itself. The EEC proposed for Ti–25Mo alloy closely simulates the formation of a compact layer with a polarization resistance (R_1) and a capacitance (CPE_1). In contrast, the EEC proposed for CP-Ti simulates the formation of oxide layer that consists of a barrier-like inner layer and a porous outer layer. In this EEC, R_2 and R_1 are the resistances of porous and barrier layers, which are associated to the charge transfer resistance through the porous layer and the participation of adsorbed intermediates. CPE_2 corresponds to the capacitance of the porous layer while CPE_1 is related to the capacitance of the barrier layer, which seems to be associated to the double layer formation. A similar EEC was used earlier by Pan et al. [20] and Aziz-Kerrzo et al. [21] to account for the corrosion behaviour of CP-Ti. The validity of these models is confirmed based on the better non-linear least square fitting of the experimental data within 5% error. The EIS parameters determined from the Nyquist plots after fitting the data using Boukamp software are compiled in Table 1. Comparison of the resistance values of CP-Ti (19.5 ± 0.2 kΩ cm^2) and Ti–25Mo alloy (69.1 ± 0.3 kΩ cm^2) clearly reveals the improvement in corrosion resistance offered by the Ti–25Mo alloy. The Bode phase angle plots of the CP-Ti and Ti–25Mo alloy are shown in Fig. 5. The phase angle maximum of CP-Ti and Ti–25Mo alloy are −69 and −64°, respectively. Ideally, for systems which exhibit a near-capacitive behaviour the phase angle

Table 1 Corrosion parameters[a] of CP-Ti and Ti-25Mo alloy in 0.9 wt% NaCl obtained from potentiodynamic polarization and EIS studies

Type of sample	Open circuit potential (mV vs. SCE)	Passivation range (mV vs. SCE)	Passive current density (i_{pass}) ($\mu A\ cm^{-2}$)	R_1 ($k\Omega\ cm^2$)	CPE_1 (mho s^n cm^{-2}) $\times\ 10^{-5}$	n_1	R_2 ($k\Omega\ cm^2$)	CPE_2 (mho s^n cm^{-2}) $\times 10^{-4}$	n_2
CP-Ti	−407 ± 7	145−1522	32 ± 3	19.5 ± 0.2	4.13 ± 0.7	0.70	8.29 ± 0.2	5.61 ± 0.5	0.62
Ti–25-Mo	−434 ± 10	50−2530	10 ± 5	69.1 ± 0.3	10.00 ± 0.9	0.78	–	–	–

[a] Average of three 3 determinations

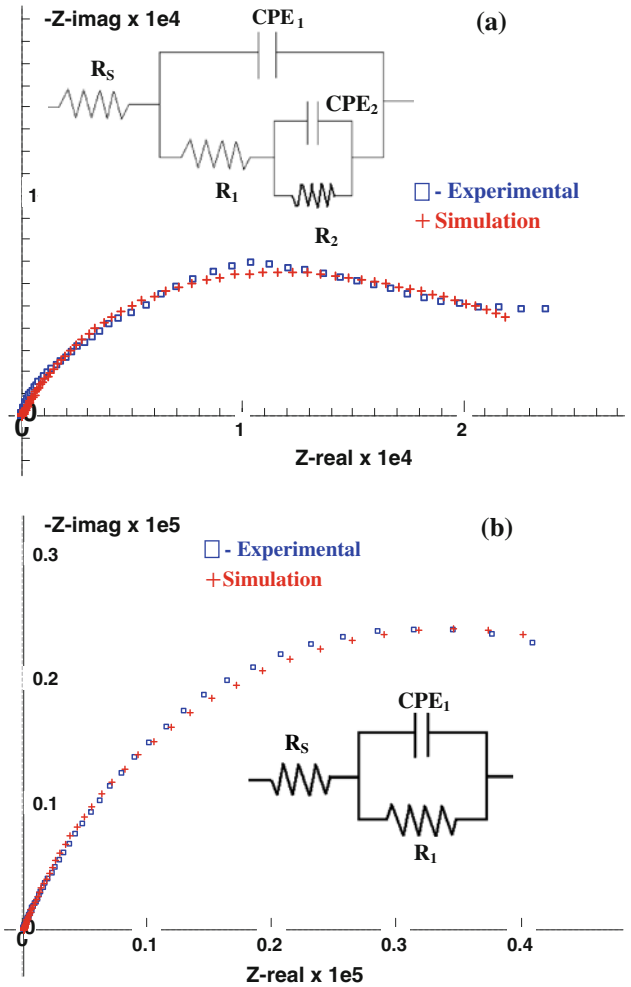

Fig. 4 Nyquist plots of CP-Ti (**a**) and Ti–25Mo (**b**) alloy in 0.9 wt% NaCl obtained at their respective open circuit potentials along with the fitting obtained and the corresponding equivalent electrical circuit [the impedance spectra were obtained using an excitation voltage of 10 mV rms (root mean square) in the frequency range between 10 kHz and 0.01 Hz]

maximum should be −90°. The lower phase angle maximum observed for CP-Ti and Ti–25Mo alloy could be due to the higher corrosivity of the medium. We have observed a similar phase angle maximum of 65–70° for Ti–15Mo alloys in 0.15 M NaCl containing varying concentrations of fluoride ions (190, 570, 1,140 and 9,500 ppm) in our earlier study [15]. The phase angle maximum of CP-Ti occurs at 20 Hz, covering a small frequency range from 18 to 9 Hz and subsequently reduces to −11° at 0.01 Hz. However, the phase angle maximum of Ti–25Mo alloy remained constant over a wide range of frequency in the lower frequency side i.e. from 4 to 0.1 Hz and subsequently reduces to−30° at 0.01 Hz. The occurrence of a constant phase angle maximum over a wide frequency range for Ti–25Mo alloy suggests the formation of a stable passive oxide film and the difficulty in charge transfer process. The decrease in the phase angle shift observed for CP-Ti and Ti–25Mo alloy after 9 and 0.1 Hz, respectively is due to the dissolution of the oxide layer.

Microstructural studies indicate the presence of equiaxed α-grain with some twin bands for CP-Ti whereas β-grains are the only dominant phase in Ti–25Mo alloy in which the β-grains are homogeneous and evenly distributed. The homogeneous distribution of the β-grains enables Ti–25Mo alloy to offer a better corrosion resistance. Potentiodynamic polarization studies reveal that Ti–25Mo alloy offers a relatively larger passive range (from +50 to 2530 mV vs. SCE) and lower passive current density (10 $\mu A\ cm^{-2}$) compared to that of CP-Ti (from +145 to +1522 mV vs. SCE and 32 $\mu A\ cm^{-2}$) in 0.9 wt% NaCl. The constant phase angle maximum, observed over a wide range of frequency (from 4 to 0.1 Hz), in the Bode phase angle plot of Ti–25Mo alloy supports the large passive range and lower passive current density observed in polarization studies, thus confirming the formation of a stable passive oxide film and the difficulty in charge transfer process of Ti–25Mo alloy. The results of the potentiodynamic polarization and EIS studies reveal that Ti–25Mo alloy offers a better corrosion resistance than CP-Ti in 0.9 wt% NaCl and it appears be a better choice for orthopaedic implant applications.

4 Conclusions

Ti–25Mo alloy exhibits β-grains as the only dominant phase which is homogeneous and evenly distributed. Ti–25Mo alloy exhibits a higher passivation range and lower i_{pass} in 0.9 wt% NaCl, suggesting its better corrosion protective ability compared to that of CP-Ti. The phase angle maximum of CP-Ti and Ti–25Mo alloy are quite similar. However, the phase angle maximum of Ti–25Mo

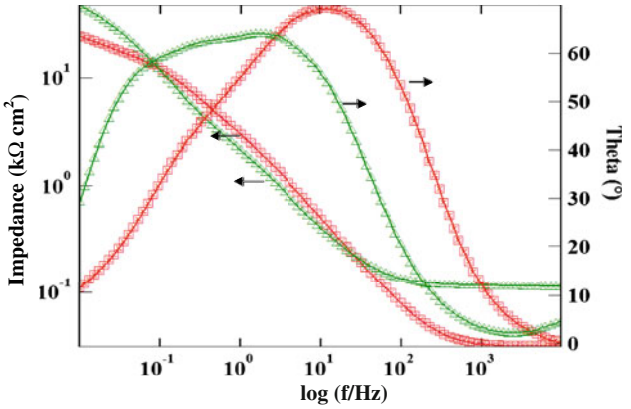

Fig. 5 Bode plots of CP-Ti (×) and Ti–25Mo (△) alloy in 0.9 wt% NaCl obtained at their respective open circuit potentials [the impedance spectra were obtained using an excitation voltage of 10 mV rms (root mean square) in the frequency range between 10 kHz and 0.01 Hz]

alloy remained constant over a wide range of frequency in the lower frequency side, which indicates a better stability of the passive oxide film and the difficulty in charge transfer process. The study reveals that Ti–25Mo alloy could offer a better corrosion resistance than CP-Ti in 0.9 wt% NaCl and from corrosion protection point of view it appears be a better choice for orthopaedic implant applications.

Acknowledgments The authors express their sincere thanks to Dr. T. Nishimura of NIMS, Japan for providing them with the gift samples of Ti–25Mo alloy. The authors thank Dr. S. Srikanth, Director, National Metallurgical Laboratory, Jamshedpur, for his keen interest and permission to publish this paper.

References

1. Kovacs P, Davidson JA (1996) Chemical and electrochemical aspects of the biocompatibility of titanium and its alloys. In: Brown SA, Lemons JE (eds) Medical applications of titanium and its alloys: the materials and biological issues. ASTM STP 1272, Philadelphia, p 163
2. Fonseca C, Barbosa MA (2001) Corros Sci 43:547
3. Ho WF, Ju CP, Lin HC (1999) Biomaterials 20:2115
4. Ho WF (2008) J Alloys Compd 464:580
5. Nag S, Banerjee R, Fraser HL (2005) Mater Sci Eng C 25:357
6. Nag S, Banerjee R, Fraser HL (2005) J Mater Sci Mater Med 16:679
7. Oliveira NTC, Aleixo G, Caram R, Guastaldi AC (2007) Mater Sci Eng A 452–453:727
8. Oliveira NTC, Guastaldi AC (2008) Corros Sci 50:938
9. Oliveira NTC, Guastaldi AC (2009) Acta Biomater 5:399
10. Habazaki H, Uozumi M, Konno H, Shimizu K, Nagata S, Asami K, Skeldon P, Thompson GE (2002) Electrochim Acta 47:3837
11. Habazaki H, Uozumi M, Konno H, Shimizu K (2003) Surf Coat Technol 169-170:151
12. Karthega M, Raman V, Rajendran N (2007) Acta Biomater 3:1019
13. Alves APR, Santana FA, Rosa LAA, Cursino SA, Codaro EN (2004) Mater Sci Eng C 24:693
14. Capela MV, Acciari HA, Capela JMV, Carvalho TM, Melin MCS (2008) J Alloys Compd 465:479
15. Kumar S, Sankara Narayanan TSN (2008) J Dent 36:500
16. Kumar S, Sankara Narayanan TSN (2009) J Alloys Compd 479:699
17. Ramires I, Guastaldi AC (2002) Quím Nova 25:10
18. Davis R, Flower HM, West DRF (1979) J Mater Sci 14:712
19. Bania PJ (1993) Beta titanium alloys and their role in the titanium industry. In:beta titanium alloys in the 1990s. The Mineral Metals and Materials Society, Warrendale, p 3
20. Pan J, Thierry D, Leygraf C (1996) Electrochim Acta 41:1143
21. Aziz-Kerrzo M, Conroy KG, Fenelon AM, Farrell ST, Breslin CB (2001) Biomaterials 22:1531